TECHNICAL TRANSACTIONS 2/2018
ENVIRONMENTAL ENGINEERING
DOI: 10.4467/2353737XCT.18.029.8002
SUBMISSION OF THE FINAL VERSION: 22/1/2018

Bernard Twaróg (btwarog@pk.edu.pl)
Institute of Hydraulic Engineering and Water Management, Department of Hydraulic Engineering and Water Management, Faculty of Environmental Engineering, Cracow University of Technology

Interaction between hydraulic conditions and structures – fluid structure interaction problem solving. A case study of a hydraulic structure

Interakcja warunków hydraulicznych oraz konstrukcji – rozwiązywanie problemów FSI na przykładzie obiektu hydrotechnicznego

Abstract

Contemporary analytical and computational techniques enable the researcher to define interaction between varying flow rates, varying volumes of filling water and the deformation and stresses occurring in the structural components of a hydraulic structure. This study aims to describe and create visualisations, under selected operating conditions, of displacements, deformations and stresses of a hydraulic structure resulting from loads generated by hydraulic conditions in standard components of the structure. A sample analysis was carried out for the Niedów earthen dam on the Witka River that failed in 2010 due to a disastrous inflow. The scope of this analysis covers the components of the spillway section: the spillway monolith, the dissipation basin slab and the flip bucket. The results of analytical work and visualisations are shown using the Flow3D software program.

Keywords: hydraulic structure, CFD, stresses, deformations, displacements, spillway section, disaster, FSI solving

Streszczenie

Współczesne techniki analiz i obliczeń pozwalają na określenie wzajemnej interakcji pomiędzy zmienną wielkością przepływu i napełnienia a odkształceniem i naprężeniem, występującymi w elementach konstrukcyjnych obiektu hydrotechnicznego. Tematem proponowanego artykułu, dla wybranych warunków pracy obiektu hydrotechnicznego, jest opis i wizualizacja przemieszczeń, odkształceń oraz naprężeń będących konsekwencją obciążeń generowanych warunkami hydraulicznymi dla typowych elementów obiektu hydrotechnicznego. Przykład analizy został opracowany dla zapory ziemnej Niedów na rzece Witce, która uległa awarii w 2010 roku wskutek katastrofalnego dopływu. Zakres analizy obejmuje elementy sekcji przelewowej: monolit przelewu, płyta niecki wypadowej oraz szykany. Wyniki analiz i wizualizacje są prezentowane z wykorzystaniem oprogramowania Flow3D.

Keywords: obiekt hydrotechniczny, CFD, naprężenia, odkształcenia, przemieszczenia, sekcja przelewowa, katastrofa, rozwiązywanie FSI

1. An introduction to the FSI problems

Interactions between the motions of incompressible fluids and structures immersed in them represent non-linear physics problems that are investigated in a wide scope of scientific and engineering disciplines.

This study discusses the rules for the computation of components of a hydraulic structure affected by the motions of water and presents selected, representative operational examples. A model was developed for extreme operating conditions of the structure; boundary conditions were defined and a sample interaction between the hydraulic structure and the medium (FSI – Fluid Structure Interaction) was analysed using numerical methods.

In interactions between a fluid and a structure, the effects of the surrounding fluid on the structure may be exerted from the inside, from the outside or from both. Contemporary science and engineering studies heavily focus on research into the effects of surrounding fluids on structures and place great emphasis on the description and solving of strongly non-linear and multi-disciplinary problems of FSI (Chakrabarti, 2005; Dowell & Hall, 2001; Morand & Ohayon, 1995).

For most FSI problems, analytical solutions cannot be identified; furthermore, the space for conducting experiments in the laboratory is limited. Therefore, the main emphasis for research is placed on the application and development of numerical methods.

The use of computer techniques in solving FSI problems brings new possibilities on a near daily basis; more effective algorithms have been developed and solved which describe the behaviour of more complex structural designs and interactions between fluids and structures.

Sample applications of FSI are not limited to hydrodynamics and problems of structural dynamics. FSI methods are widely applied in research into bed load transport and sedimentation (Mucha et al., 2004; Tornberg & Shelley, 2004; Wang & Layton, 2009), aerodynamics (Haase, 2001; Zhang Jiang & Ye, 2007), turbulence (Kaligzin & Iaccarino, 2003; Yang & Balaras, 2006), medium flow in irregular geometries (Fadlun et al., 2000; Udaykumar et al., 1996, 2001), electrohydrodynamics (Hoburg & Melcher, 1976), magnetohydrodynamic flows (Grigoriadis et al., 2009), and descriptions of the behaviour of bio-fluids or biomechanics (cell junction and deformation, interaction of blood with the cardiac muscle, the behaviour of the inner ear, the behaviour of jellyfish, the mobility of spermatozoa and many other problems).

The numerical procedures aimed at solving FSI problems may be divided into two approaches – a comprehensive approach and a phased approach. Certainly, both approaches are variously perceived by scientists representing various disciplines.

The comprehensive approach (Hubner et al., 2004; Michler et al., 2004; Ryzhakov et al., 2010) describes fluid dynamics and structures using the same mathematical frameworks, proposing one equation system for the entire problem which is solved using a single algorithm. This approach may potentially achieve greater accuracy in defining interdisciplinary problems but may also require considerable computing power and greater resources and knowledge in order to develop and maintain a highly specialist code.

Unlike the comprehensive approach, the phased approach considers the fluid and the structure in separate computational domains, and in two separated and disjointed numerical meshes and computational algorithms.

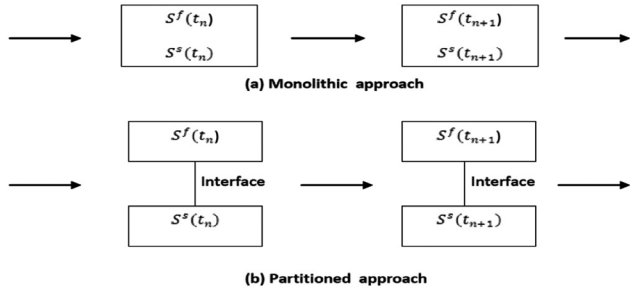

Fig. 1. A schematic diagram of the comprehensive and phased approaches in FSI problem solving [5]

Other generalised approaches are used that are based on the application of matching/conforming and non-matching/nonconforming meshes. The application of matching meshes is dependent upon using meshing methods that take into account the shape of the object (a structure, solid body) and the variation of boundary conditions. Repeated meshing is required to represent motions and deformations of the structure, using a matching or a non-matching mesh.

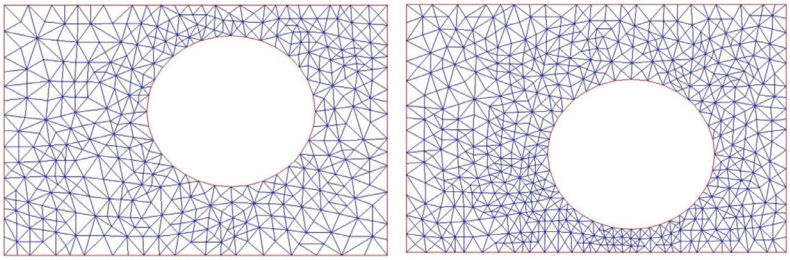

Fig. 2. Sample matching meshes for various times, t_1 and t_2

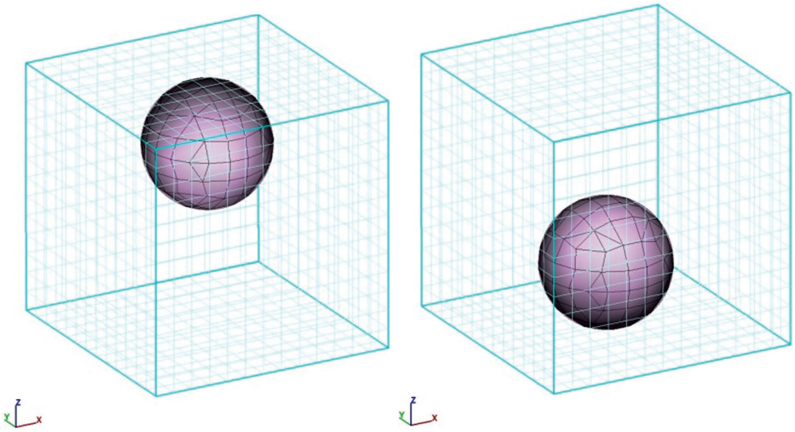

Fig. 3. Sample non-matching meshes for various times, t_1 and t_2

2. FSI problem definition

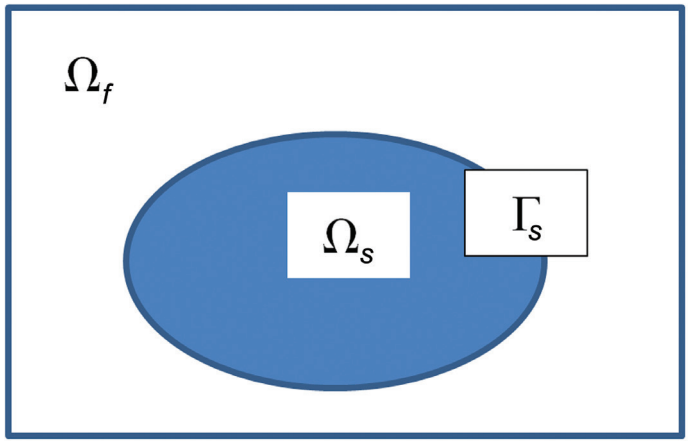

Fig. 4. A schematic diagram of the solid body, fluid domains and the interface domain

Let us assume a computational domain and mark it as Ω with an external boundary Γ. Let the analysed domain contain the area of a rigid body (the structure) Ω_S and the area of fluid Ω_f.

$$\Omega = \Omega_s \cup \Omega_f$$

The area of joint effect of the fluid and the rigid body is defined by the condition

$$\Gamma_s = \Omega_s \cap \Omega_f$$

The equations representing motions of the fluid and the rigid body may be formulated using previously adopted indices and the d'Alembert's principle:

$$p\dot{v}_i - \sigma_{ij,j} + f_i = 0 \qquad \text{Eq. 2.1}$$

where:

f_i – gravity forces

The equation in the solid body domain may be formulated as:

$$\rho^s \dot{v}_i^s - \sigma_{ij,j}^s + f_i^s = 0 \text{ w obszarze } \Omega_S \qquad \text{Eq. 2.2}$$

Consider that the velocity $\dot{v}_i^s$ is a time derivative of the displacement field u_i^s thus:

$$v_i^s = \dot{u}_i^s$$

The first two terms of equation 2.2 describe inertia and the internal stress state, respectively.

For example, when describing the behaviour of a rigid body in the domain of linear deformations using Hooke's law to calculate the stresses, we obtain:

$$\sigma_{ij}^{s} = \lambda \delta_{ij} \varepsilon_{11} + 2G\varepsilon_{ij}$$

where:

σ_{ij}^{s} – the tensor of stresses in the rigid body is expressed as a tensor of deformations and Lamé constants defined by the following equations:

$$\varepsilon_{ij} = \frac{1}{2}(u_{ij} + u_{ji})$$

$$G = \frac{E}{2(1+\nu)}$$

$$\lambda = \frac{E\nu}{(1+\nu)(1-2\nu)}$$

where:

E – Young's modulus,

ν – Poisson's ratio.

In the fluid domain, the equations may be formulated as follows:

$$\rho^{f} \dot{v}_{i}^{f} - \sigma_{ij,j}^{f} + f_{i}^{f} = 0 \text{ in the region of } \Omega_{f} \qquad \text{Eq. 2.3}$$

Internal conditions may be defined as:

$$\dot{v}_{i}^{f} = \frac{dv_{i}^{f}}{dt} = \frac{\partial v_{i}^{f}}{\partial t} + v_{j}^{f} v_{ij}^{f}$$

Assuming incompressible fluids and Newtonian stresses in the fluid, we obtain:

$$\sigma_{ij}^{f} = -p\delta_{ij} + \tau_{ij}$$

where:

$$\tau_{ij} = 2\mu\left(e_{ij} - \delta_{ij}\frac{e_{kk}}{3}\right)$$

$$e_{ij} = \left(v_{ji}^{f} + v_{ij}^{f}\right)$$

Consider that represents the hydrostatic pressure that may be understood *to be in an enforced state* of incompressibility:

$$v_{i,i}^{f} = 0$$

It is often assumed in fluid mechanics that fluid particles do not move at the boundary (the no-slip condition). A viscous fluid has a velocity of zero relative to the boundary

represented by the surface of a solid body during flow. Note that this condition along the interface area of the fluid and solid body surfaces may be defined as follows, using the Dirichlet and von Neumann boundary conditions:

$$v_i^s = v_i^f \text{ na } \Gamma_s \qquad \text{Eq. 2.4}$$

$$\sigma_{ij}^s n_i = \sigma_{ij}^f n_i \text{ na } \Gamma_s \qquad \text{Eq. 2.5}$$

Under real conditions, the differentiation of the displacement conditions in both domains leads to the domain interface equation

$$x_i^s = x_i^f \text{ na } \Gamma_s \qquad \text{Eq. 2.6}$$

3. Matching mesh methods

The matching mesh methods applied to solve FSI problems usually cover three areas: fluid dynamics, solid body motion dynamics and the mesh. The sequence of solving is intuitively comprehensible. Firstly, the equations for the fluid field may be solved for a given moment and specific location of the solid body. The calculated pressure and stress values are related to the solid body and to the external forces. Finally the behaviour of the solid body is calculated and a new mesh is then generated that matches the surface that has changed due to motion or deformation of the solid body. This iterative process may lead, at a purposefully selected time step, to the obtaining of convergent solutions.

4. Flow 3D software

Flow3D is a computer program that uses non-matching mesh methods to solve the FSI problems. It is designed to generate and solve fluid-structure interaction (FSI) problems and provides a platform that includes both fluid flow and solid body mechanics factors.

In the solid-body domain, the FSI module uses the finite element method (FEM) to simulate and analyse stresses and deformations. The stresses in the solid body are caused by external forces exerted on it by the surrounding fluid or by other limitations or constraints imposed on it.

5. Preprocessing – FSI modelling

It is enough to select the FSI option to activate the FSI module in the elements describing the properties of individual components. The choice must be finalised by entering material properties such as the density of the solid body and at least two of the following parameters:

the Young's modulus, the bulk modulus of elasticity, the shear modulus, the yield point, the Poisson's ratio.

Entering the yield point activates a material effort model that predicts local plastic deformations in the locations where the yield point is exceeded by stresses that are calculated according to von Mises theory.

The next step following the definition of material properties consists of the generation of a mesh of finite elements that discretises the solid body domain. By default, the preprocessor uses a Cartesian mesh defined to describe the fluid domain, but local meshes of finite elements may also be generated to describe the solid body.

The FSI model gradually solves the equations of solid body dynamics, so that it is theoretically capable of predicting major deformations with an adequate level of accuracy; however, fluid motions due to displacements at the boundary of the fluid and solid body phases are not updated. Consequently, the mapped dynamics of the solid body have no effect on the fluid behaviour in simulation results when modelling major deformations.

In the current version, the components of the solid body need to be limited by the boundaries of the fluid mesh or by contacts with other components so that motions of those components do not need to be mapped in the behaviour of the surrounding fluid. Therefore, the model must currently be structured so that motions of the components are appropriately limited (i.e. constraints must be imposed on them) in order to obtain a correct simulation.

6. Postprocessing – FSI modelling

The results of modelling of the rigid body behaviour may be viewed separately in the Flow3D interface by selecting the type of rigid body component and the result of calculations using finite elements. The user may select displacements, deformations and stresses along the axis of the adopted coordinate system.

Initially, the interface proposes a visualisation of normal displacements. These are defined as displacements of elements of the solid body surface (positive or negative) in the normal direction of this surface. Negative values of normal displacements present a visualisation of compression; positive values result from expansion. Six components of the deformation and stress tensor may additionally be visually represented.

An averaged value of stresses (ISO – an isotropic state) and stresses calculated according to von Mises theory may also be visually represented.

7. The concept of FSI modelling in Flow3D

Interaction between a fluid and a solid body (FSI – Fluid Structure Interaction) is modelled in Flow3D using fully coupled equations describing the dynamics of the solid body and the behaviour of the fluid. The approach used is not designed only to solve the flow problem. No

finite difference mesh is used in this module; it is replaced with a matching mesh of finite elements that is warped with the solid body.

This solution *is typically adopted* because the equations of solid mechanics are more convenient by far when solving solid body problems.

The current Flow3D software version enables the user to generate a new mesh of finite elements that matches the solid body – it is capable of providing a description of the solid body domain using a tetragonal or hexagonal mesh. The contact area (the interface) between the fluid and the solid body is processed so as to match the nodes of the external mesh with the mesh describing the solid body. The nearest nodes of the external mesh are matched with the nodes located on the solid body surface using the criterion of distance along the normal line to the surface of the solid body.

In certain cases, adjacent nodes are combined or selected nodes are removed.

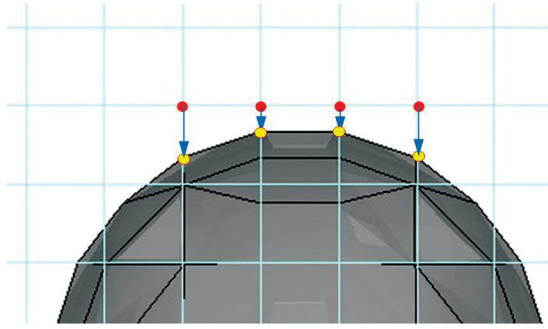

Fig. 5. The diagram represents a simplified 2D version of the problem of 'pulling' the nodes of the external mesh towards the nodes of the solid body mesh

The diagram shows a simplified version of the node pulling process. The developers of the program adopted the philosophy of a fully automated node matching process without external adjustment by the user.

8. The equations used in the Flow3D software

The basic equation used to describe motion of a rigid body is the d'Alembert principle:

$$\rho\frac{d^2x}{dt^2}=\nabla\boldsymbol{\sigma}+\rho\boldsymbol{b} \qquad \text{Eq. 8.1}$$

where:

- ρ – density of the rigid body,
- t – time,
- x – point coordinates,
- $\boldsymbol{\sigma}$ – Cauchy stress tensor,
- $\boldsymbol{b}$ – body forces.

The stress tensor is a measure of the stress state in a rigid body; it is related to material deformations and to other internal stresses in a rigid body – the program also enables the user to solve the problem of stresses caused by thermal phenomena. Deformation is a measure of the physical distortion affecting the body and is also represented by a tensor.

The approach adopted in this study is based on minor, gradual deformations. Consequently, the increment of deformation in one time step is calculated using the following formula:

$$E' = \frac{1}{2}\left\{[\nabla(\delta x)]^T + \nabla(\delta x)\right\} = \frac{1}{2}\left[\frac{\partial(\delta x)_i}{\partial x_j^n} + \frac{\partial(\delta x)_j}{\partial x_j^n}\right] e_i e_j \qquad \text{Eq. 8.2}$$

where:

E' – increment of deformation,
i, j – indices describing Cartesian coordinated in the directions,
e_i – unit vector in the system,
δx – describes the displacement vector.

$$\delta x = x^{n+1} - x^n \qquad \text{Eq. 8.3}$$

where:

x^n – represents the location of the point in the preceding rigid body at the moment,
x^{n+1} – represents the location of the point in the rigid body at the moment.

The Couchy stress tensor for the moment $n + 1$, σ^{n+1}, is calculated based on Hooke's linear model:

$$\sigma^{n+1} = \sigma^n + \left(K - \frac{2}{3}G\right) tr(E') + 2GE' \qquad \text{Eq. 8.4}$$

where:

$n, n + 1$ – represent time indices,
K – bulk modulus of elasticity,
G – shear modulus,
$tr(E')$ – the trace of the deformation tensor, i.e. the sum of its components on the main diagonal.

The bulk modulus of elasticity describes the resistance of an isotropic body to volume changes when the body is subject to isometric compression or expansion. The shear modulus describes the resistance of the body to shear. Both modulus forms are obtained from a functional dependence of the elasticity module and Poisson's ratio.

The FSI module in Flow3D is executed when a combination of at least two elements is given in material parameters.

The algorithm uses dependencies between material constants:

$$K = \frac{E}{3(1-2\nu)}, \quad G = \frac{E}{2(1+\nu)} \qquad \text{Eq. 8.5}$$

The acceleration conditions (8.1) are solved based on the locations of points on the body at various times:

$$\rho\frac{d^2x}{dt^2}=\rho\left(\frac{x^{n+1}-2x^n+x^{n-1}}{\Delta t^{n+1}\Delta t^n}\right) \qquad \text{Eq. 8.6}$$

9. The finite element method used in Flow3D

The equation (8.1) contains three-dimensional differential equations, solved at each time step, where x^{n+1} are unknown (σ^{n+1} are calculated directly from x^{n+1} and previous values σ in the equation 8.2). In the finite element method (FEM), the weighted remainder method is used to solve the equation (8.1). The method may be formulated as:

$$0=\int_\Omega \boldsymbol{\Psi}\left[\nabla\sigma^{n+1}+\rho\boldsymbol{b}-\rho\left(\frac{x^{n+1}-2x^n+x^{n-1}}{\Delta t^{n+1}\Delta t^n}\right)\right]d\Omega \qquad \text{Eq. 8.7}$$

where:

$\boldsymbol{\Psi}$ – the function of weights in the domain Ω.

By differentiating and minimising the formula:

$$\nabla(\boldsymbol{\Psi}\sigma^{n+1})=\boldsymbol{\Psi}\nabla\sigma^{n+1}+\nabla\boldsymbol{\Psi}\sigma^{n+1} \qquad \text{Eq. 8.8}$$

we obtain from the equations (8.7, 8.8):

$$0=\int_\Omega\left[\boldsymbol{\Psi}\nabla\sigma^{n+1}-\boldsymbol{\Psi}\rho\boldsymbol{b}+\boldsymbol{\Psi}\rho\left(\frac{x^{n+1}-2x^n+x^{n-1}}{\Delta t^{n+1}\Delta t^n}\right)\right]d\Omega-\int_\Omega\nabla(\boldsymbol{\Psi}\sigma^{n+1})d\Omega \qquad \text{Eq. 8.9}$$

The conditions on the right side of (8.9) may be recorded using Green's theorem:

$$0=\int_\Omega\left[\boldsymbol{\Psi}\nabla\sigma^{n+1}-\boldsymbol{\Psi}\rho\boldsymbol{b}+\boldsymbol{\Psi}\rho\left(\frac{x^{n+1}-2x^n+x^{n-1}}{\Delta t^{n+1}\Delta t^n}\right)\right]d\Omega-\oint\mathbf{n}(\boldsymbol{\Psi}\sigma^{n+1})d\Gamma \qquad \text{Eq. 8.10}$$

In the equation (8.10), $\boldsymbol{n}$ represents a normal vector pointing to the outside of the surface of domain , represents an infinitesimal portion of the solid body domain that constitutes the boundary domain. The indices n–1, n, and n+1 describe the time for each variable analysed. The last condition on the right side is non-zero at the boundary of the analysed domain. The weight function $\boldsymbol{\Psi}$ consists of a series of basic functions that differ from zero only around the point on the solid body they refer to and equal zero in all other points. Consequently:

$$\boldsymbol{\Psi}(x)=\sum_{i=1}^{nnodes}\psi_i \qquad \text{Eq. 8.11}$$

where:

nnodes – total number of nodes in the mesh used to discretise the domain,

x – coordinate of the point in the adopted frame of reference,

Ψ_i – represents the local values of the weight function close to the node.

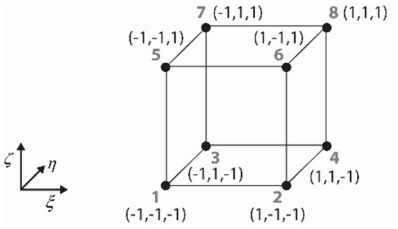

Fig. 6. Sample element of a tetragonal mesh

Let us assume a domain whose vertices correspond to 8 nodes, as in Fig. 6. The values of function Ψ_i corresponding to those nodes are non-zero while all the remaining nodes that do not relate to this element equal zero. Thus, considering the equation (8.11), we may formulate the equation (8.10) as follows:

$$0=\sum_{k=1}^{nnodes}\int_{\Omega}\left[\nabla\psi_k\sigma^{n+1}-\psi_k\rho\boldsymbol{b}+\psi_k\rho\left(\frac{x^{n+1}-2x^n+x^{n-1}}{\Delta t^{n+1}\Delta t^n}\right)\right]d\Omega-\sum_{k=1}^{nnodes}\oint\psi_k(\mathbf{n}\sigma^{n+1})d\Gamma \quad \text{Eq. 8.12}$$

The above equation is applied to each element. Since ψ_k in the equation (8.12) are non-zero only for elements that share the node k, the equation 8.12 actually leads to the system *nnodes*, and as there are three Cartesian directions, we obtain 3 x *nnodes* equations.

The function Ψ_k is recorded for each element. The basic functions are calculated within each element using computational coordinates, regardless of element orientation.

Sample forms of the weight function:

$$\Psi_1=\frac{1}{8}(1-\xi)(1-\eta)(1-\zeta)$$

$$\Psi_2=\frac{1}{8}\xi(1-\eta)(1-\zeta)$$

$$\Psi_3=\frac{1}{8}(1-\xi)\eta(1-\zeta)$$

$$\Psi_4=\frac{1}{8}\xi\eta(1-\zeta)$$

$$\Psi_5=\frac{1}{8}(1-\xi)(1-\eta)\zeta$$

$$\Psi_7 = \frac{1}{8}(1-\xi)\eta\zeta$$

$$\Psi_8 = \frac{1}{8}\xi\eta\zeta$$

The indices describe local nodes. The basic functions are both used as weight functions and represent the position and displacement:

$$\boldsymbol{x} = \sum_{k=1}^{nnodes} \boldsymbol{x}_k \psi_k \qquad \text{Eq. 8.13}$$

$\boldsymbol{x}$ – describes the position of point in the domain solved,
$\boldsymbol{x}_k$ – refers to the value in node k,
ψ_k – represents the value of basis function in node k.

10. Boundary conditions in the solid body domain

The interaction between the fluid and the solid body domain and the evolution of the stress tensor determine boundary conditions on the solid surface. If the surface area of the solid remains in contact with the fluid, the local pressure determines the force of interaction in the equation (8.12). Consequently:

$$\boldsymbol{n}\sigma^{n+1} = -\boldsymbol{n}p_{fluid} \qquad \text{Eq. 8.14}$$

The minus sign on the right side results from the adopted convention of stress signs – a compressive stress is negative.

If the boundary surfaces of the solid body are adjacent to the fluid domain boundary, the type of boundary condition defines the conditions imposed on the solid body. The domains adjacent to the boundary walls are steady; consequently, the nodes are attached to the boundary and may not move. If the symmetry condition is met, the nodes may freely move along the boundary, but may not move to the inside or to the outside of the solid body domain. For other boundary conditions, the pressure value is used to calculate motion based on the equation (8.14).

When an FSI component comes into contact with another component (either a standard or FSI component), the interface is always fixed, i.e. the nodes on the interface do not move during simulations. Full conjugation between two FSI components does not exist for that reason.

11. Sample FSI analysis

A sample FSI analysis was carried out using a model of the Niedów dam which was destroyed in the disaster of 7 August 2010. This dam break on the Witka River resulted from a limited flow capacity due to erroneous settings of limit switches, preventing the full opening of the dam Tainter gates [6–8].

11.1. Characteristics of the analysed structure (the Niedów dam)

The Niedów impounding structure was built in 1962 on the Witka River in order to create a reservoir feeding the Turów Power Plant, the Bogatynia region and a weir power station with water. The earthen dam is located on kilometre 2.8 of the Witka River course which is a right-bank tributary of the Nysa Łużycka River, with the confluence on kilometre 167.3

The structure consisted of:

- an earthen dam
- a spillway block
- a hydroelectric plant
- a pumping station

Fig. 7. The Niedów dam and the reservoir of the town of Zgorzelec, before and after the failure

A Creager-type, three-bay spillway was used to discharge significant amounts of flood water through the impounding structure. The bays with a width of 6.70 m were closed by Tainter gates lifted with the use of roller chains. The total length of the spillways amounted to 20.10 m.

The crest of the spillway was at an elevation of 204.00 m above sea level. With an elevation of the water table in the reservoir corresponding to the normal impoundment level (NIL) of 210.0 m above sea level, the unit capacity of the spillway was defined as $q = 25.0\ m^2s^{-1}$. The elevation of the dam crest was 211.60 m above sea level, and the depth of water flowing over the crest reached around 0.4 m on the day of disaster.

A peak of 211.96 m above sea level was recorded at the Witka water-level gauge at 5:10 pm. A peak of 212.05 m above sea level occurred in the dam cross-section at 5:42 pm.

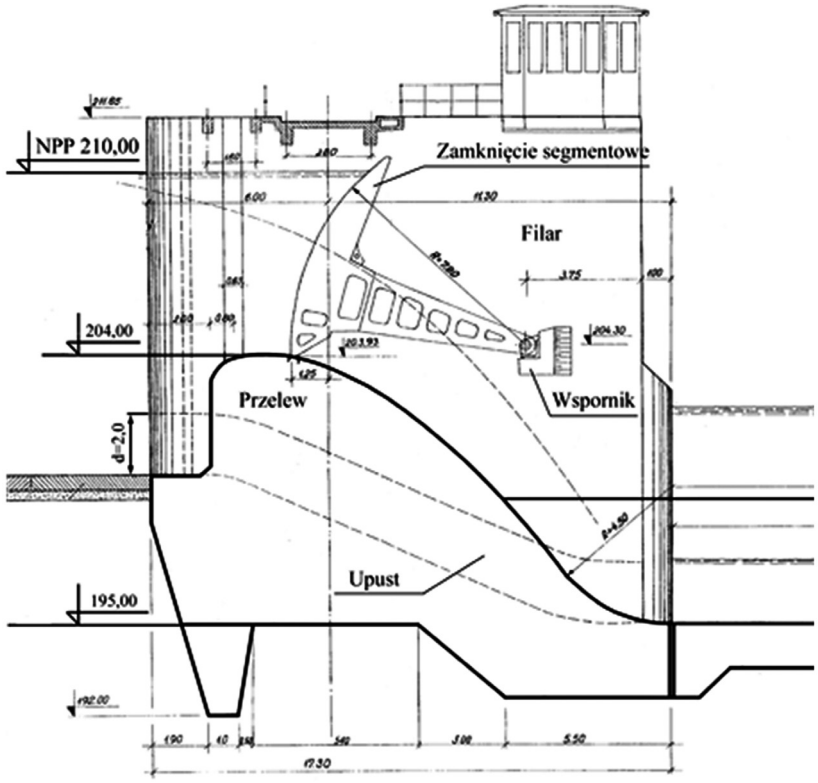

Fig. 8. Cross section of the spillways [6]

The water overflow resulted in the erosion of the downstream embankment in both dam sections; consequently, the bitumen pavement in the left dam section eroded first, then concrete facing slabs were breached and the left wing of the upstream abutment was broken off and collapsed. This caused an increase in the water outflow in the left section of the dam. Erosion of the downstream embankment occurred first in the right section of the earthen dam, then the dam increasingly eroded towards the spillway block. Water outflow caused erosion at two-thirds of the dam length to the right of the spillway block, and practically the entire dam on the left bank side. The erosion process ended at around 7:00 pm, when the reservoir was empty.

11.2. Assumptions for the FSI analysis

The following material parameters were assumed for all elements of the spillway section covered by the FSI analysis:

- material – concrete,
- density – 2300 kg/m^3,
- Young's modulus – 3.0 e+10 Pa,
- Poisson's ratio – 0.2.

The operating conditions of the structure were defined as those in place during the extreme circumstances that occurred on 7 August 2010 which led to the erosion of the dam earthen body [8]; an elevation of water table at 212.05 m above sea level was assumed. The positions of Tainter gates were set as they were at the time immediately preceding the disaster. The analysis aimed to replicate the maximum stress values that occurred in selected components of the spillway section [7, 8].

The FSI analysis was carried out for one spillway section with two boundary pillars and for the dissipation basin with the flip bucket located in the analysed section.

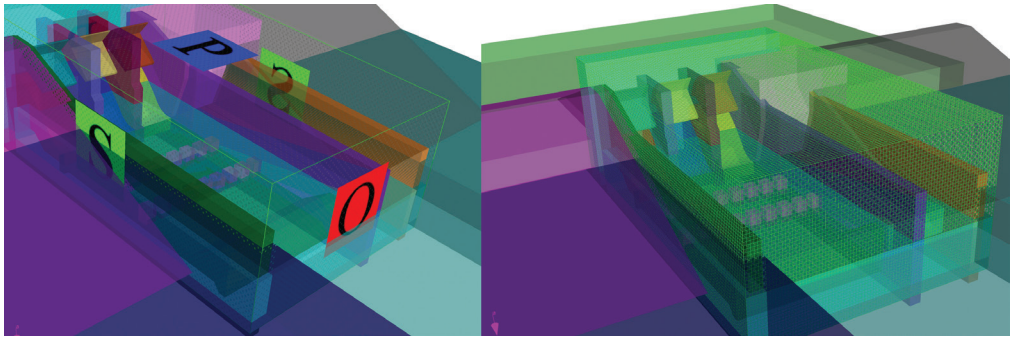

Fig. 9. Allocation of meshes used to discretise the analysed components of the spillway section [7, 8]

The modelling process was limited to the first minutes of the simulation under extreme operating conditions of the structure, preceding the moment of the erosion of the earthen body (changes in the hydraulic conditions affecting the load exerted on the structure). The meshes used to discretise the domain were allocated so as to provide nodes for the analysed components. The filtration under the structure and through the earthen body of the dam was ignored in the modelling process.

11.3. Results of the analysis

The following components of the spillway section were covered by the FSI analysis:

- the dissipation basin slab,
- the flip bucket,
- the spillway monolith.

The simulation was carried out using Flow3D software with the FSI option activated. The analysis covered deformations, stresses and displacements. The simulation model was defined for a linear range of operation of the components, in the domain described by Hooke's law.

Selected results of the analysis representing the evolution of the stress field due to the flow of breaching water in individual components of the section are given below. The selected stress states show changes in their values from a hydrostatic load until the moment of the formation of a hydraulic jump.

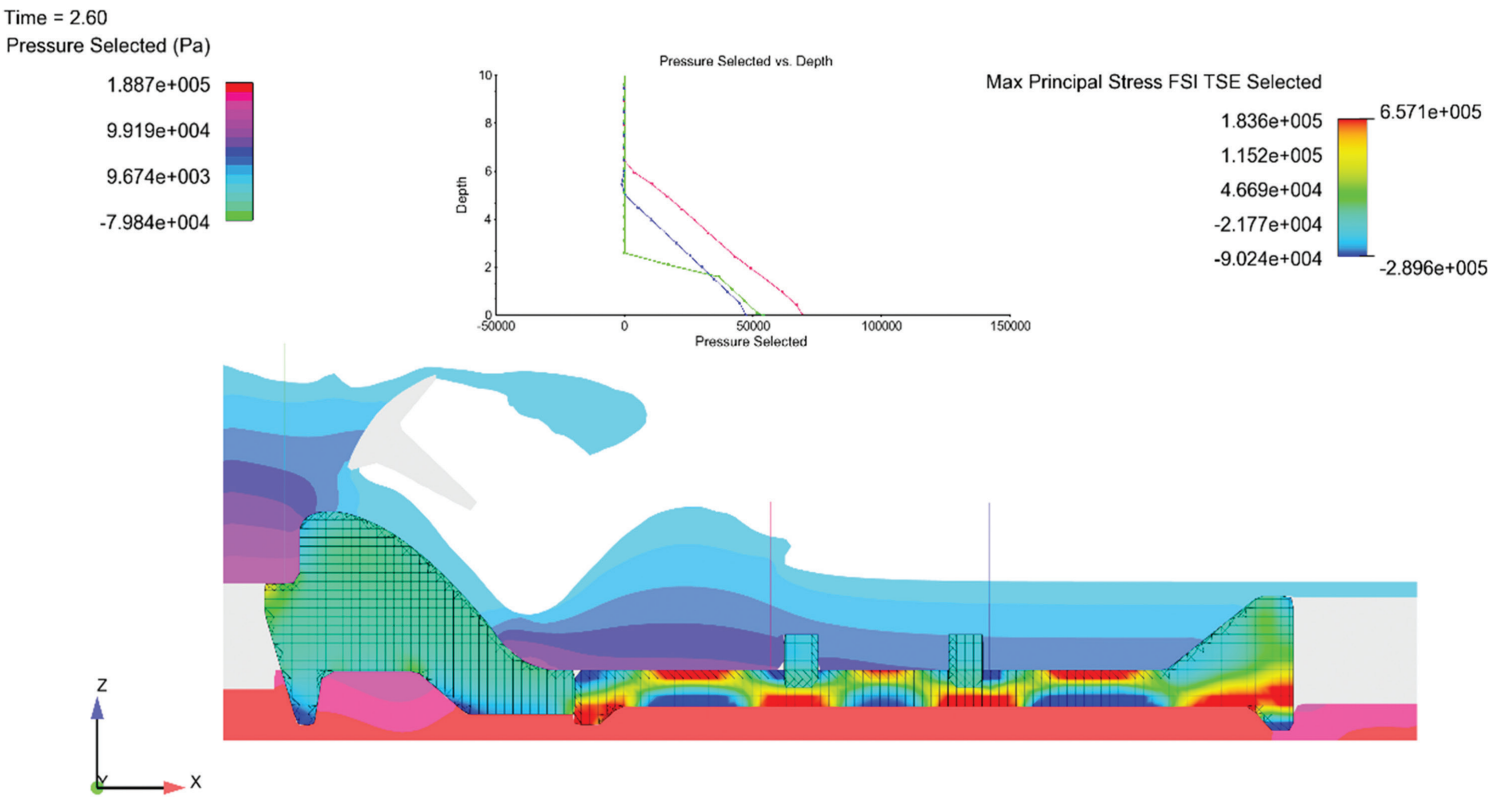

Fig. 10. Values of pressure [Pa] and maximum main stresses [Pa] in the structural components of the spillway section, $t = 2.6$ s

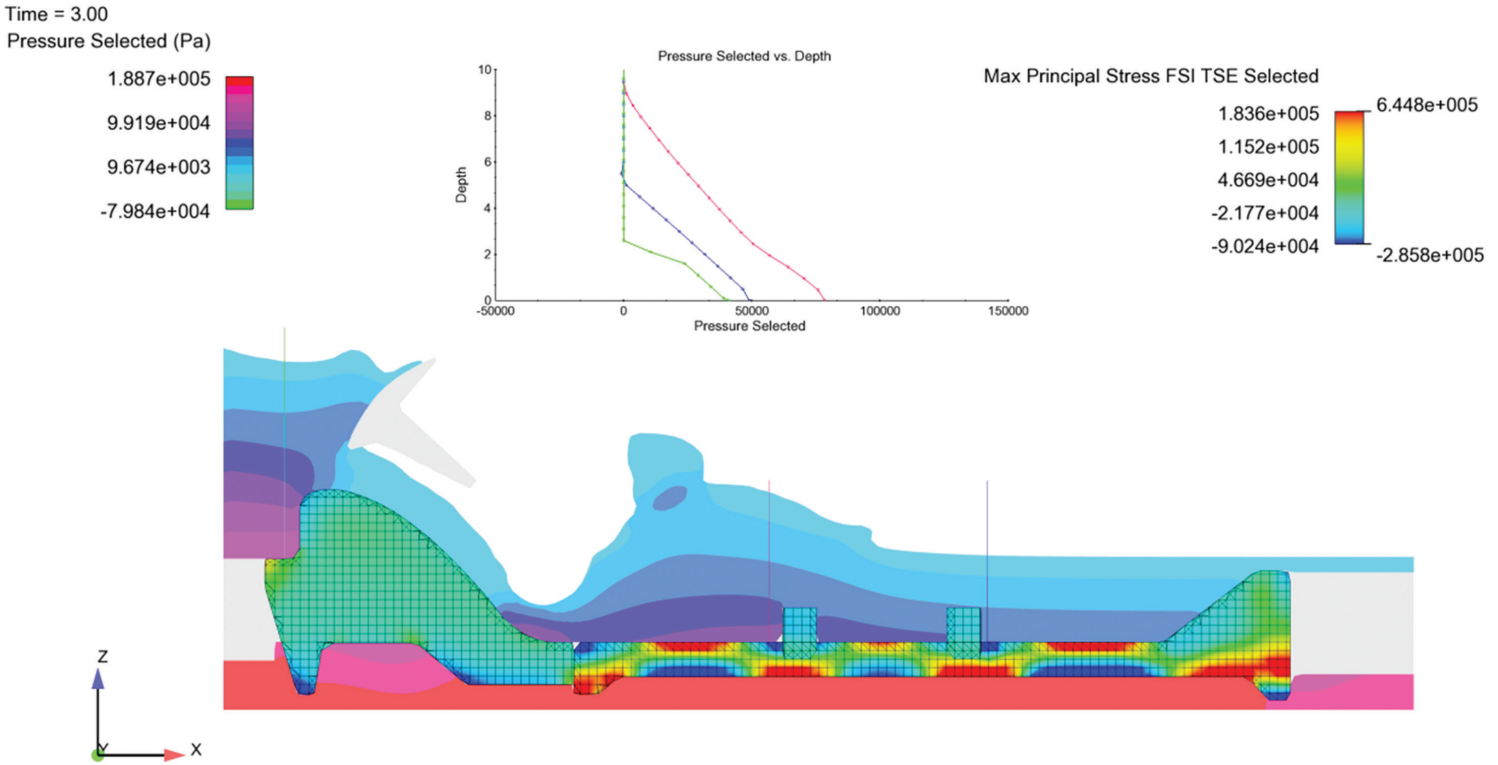

Fig. 11. Values of pressure [Pa] and maximum main stresses [Pa] in the structural components of the spillway section, t = 3.0 s

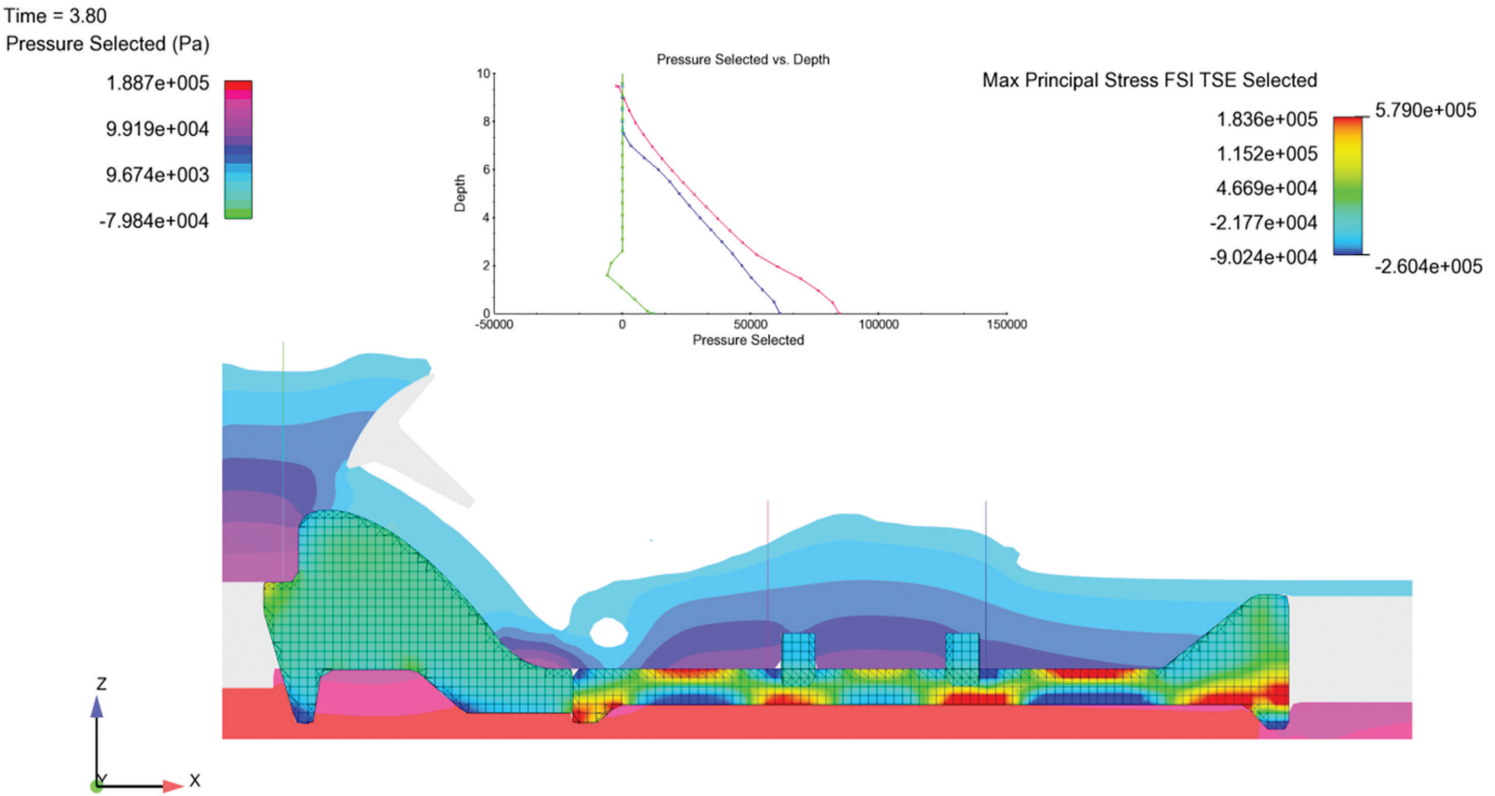

Fig. 12. Values of pressure [Pa] and maximum main stresses [Pa] in the structural components of the spillway section, $t = 3.8$ s

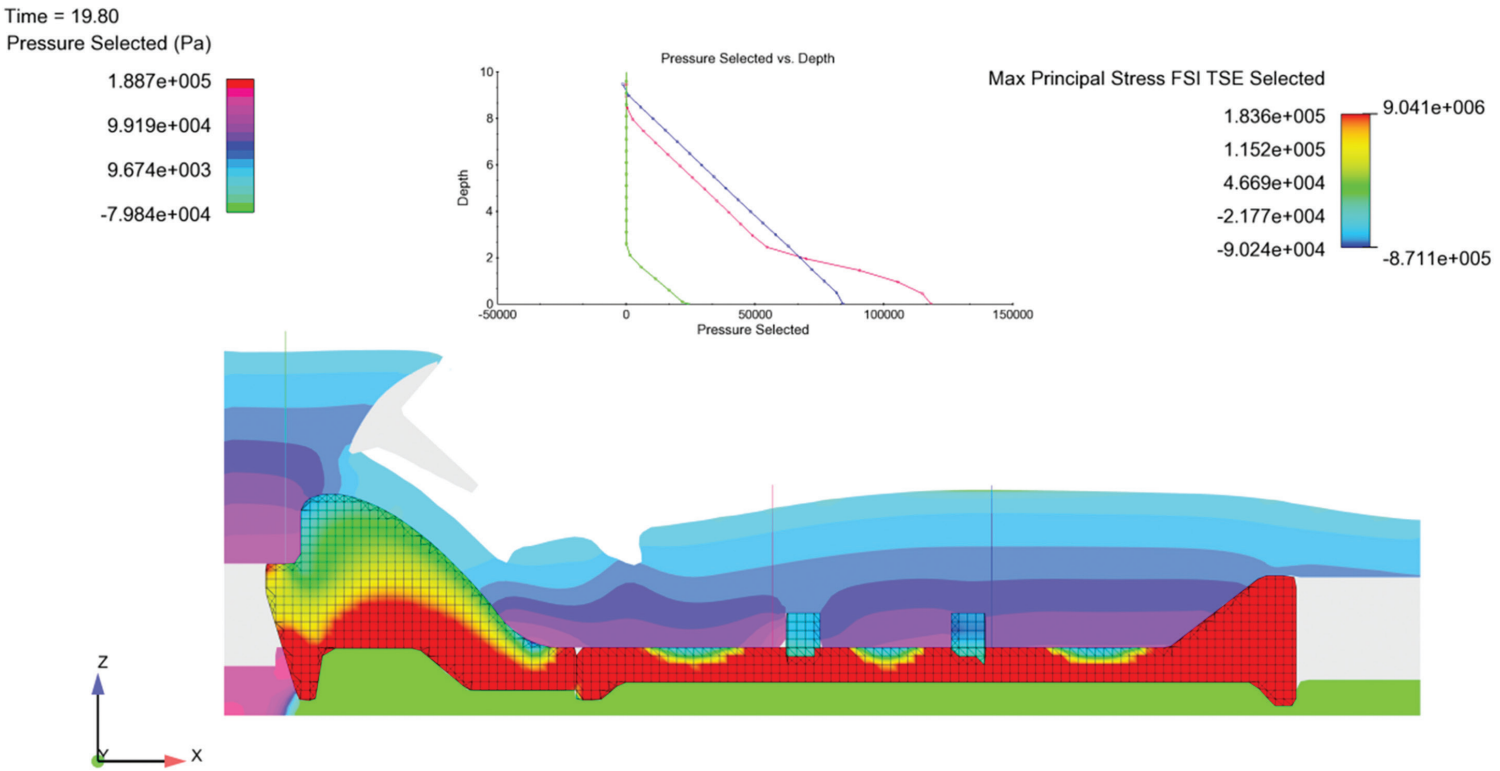

Fig. 13. Values of pressure [Pa] and maximum main stresses [Pa] in the structural components of the spillway section, $t = 20$ s

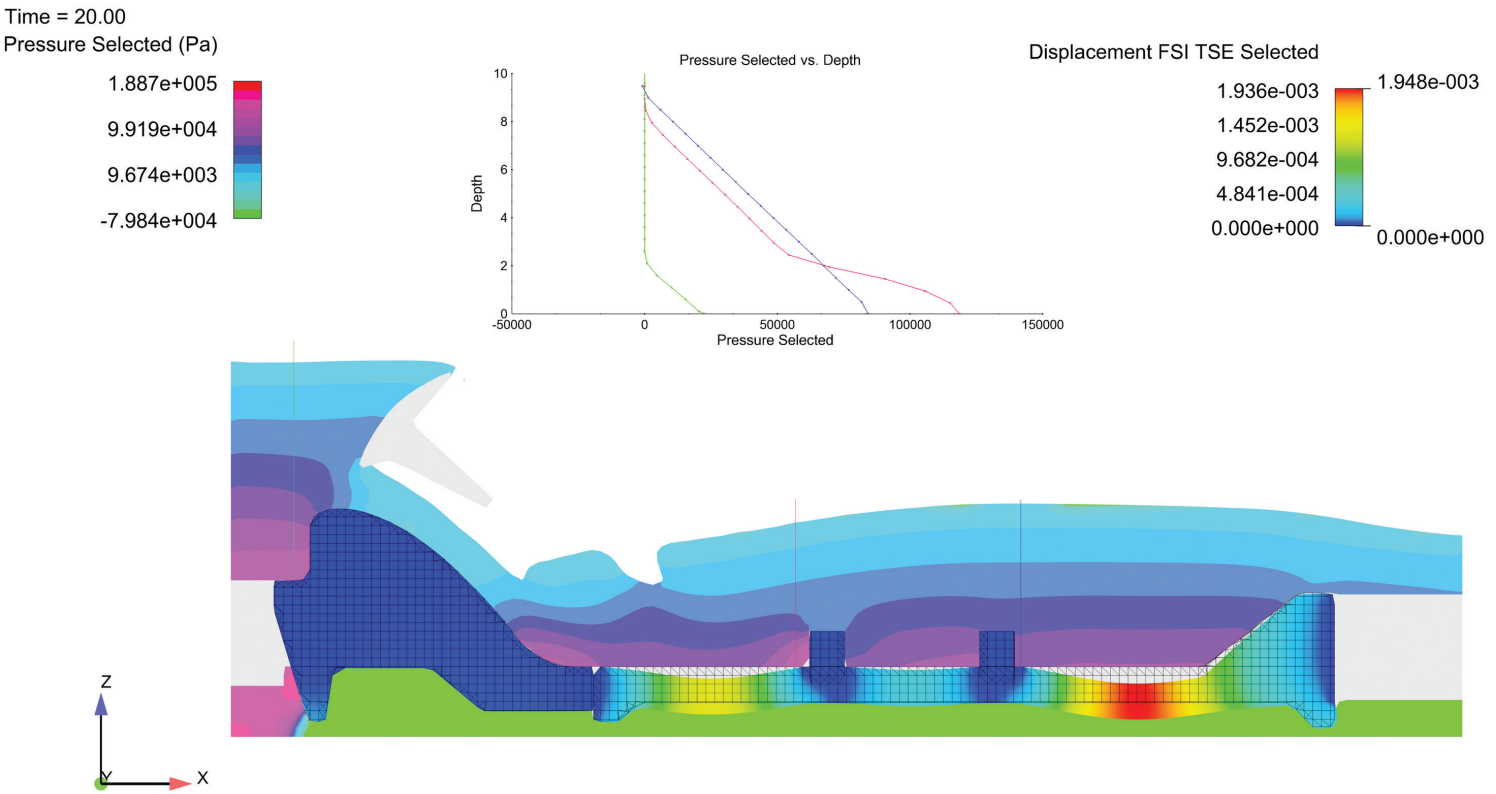

Fig. 14. Values of pressure [Pa] and values of displacements in a distorted scale [Pa] in the structural components of the spillway section, $t = 20$ s

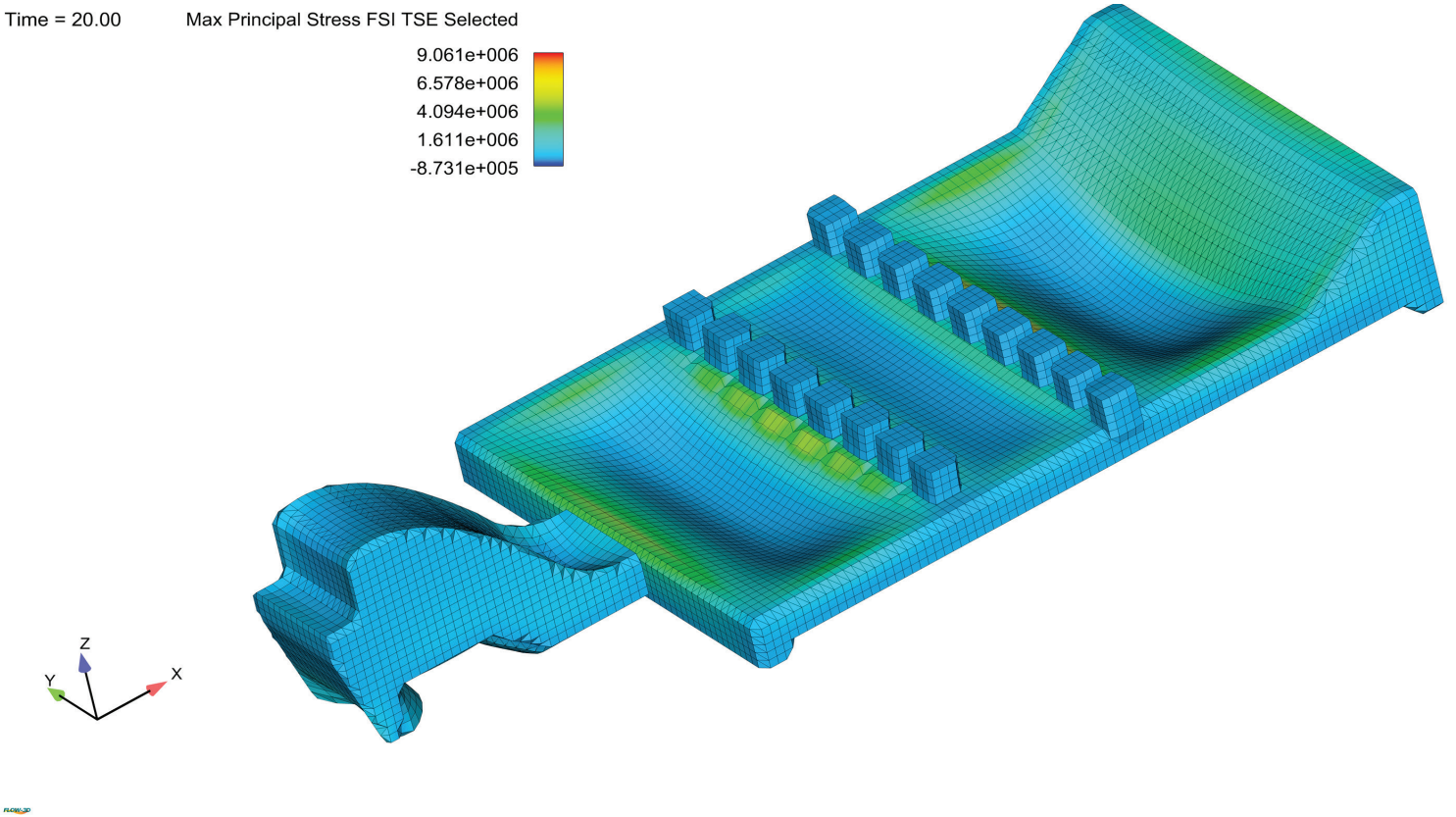

Fig. 15. Values of normal compressive and tensile stresses occurring in the spillway monolith and in the basin slab at the selected moment, $t = 20$ s

12. Conclusion

The methods and algorithms used to solve FSI problems have been dynamically developed over recent years. This development has mainly been driven by the demand observed in numerous scientific and engineering disciplines where FSI problems are identified and play an increasingly important role. A rapid increase in computation efficiency is favourable for the application of demanding calculation techniques. FSI numerical research has become a separate discipline. Due to the interdisciplinary nature of FSI problems, the development of this discipline is conditional upon contributions made by engineers and research representing various disciplines.

The completed FSI analysis of selected concrete (and reinforced concrete) components of the spillway section of the destroyed structure shows the potential of contemporary computational methods as used to identify domains subject to varying stress values.

The analysis covering the first several dozens of seconds of *see above note* the operation of the structure during a disaster resulted in the identification of two distinct phases of structural component operation in terms of stress variation. The first phase displays a considerable variation of inflow and velocity, mainly in the dissipation basin (formation of the hydraulic jump) in the spillway section, and consequently, by a considerable variation in the pressures that generate a stress state with the values of normal stresses reaching ±1e+6 Pa (Fig. 10–12). In the second phase of operation of the structure, the outflow from the basin initially stabilizes with a submerged hydraulic jump. Larger pressure, but at lower velocities, and the generated stress state is characterised by normal stress values reaching ±1e+7 Pa (Fig. 14). The conditions change over the following seconds, because the structure erodes and is finally destroyed.

Considerable variation of normal stress values and their arithmetical signs occurs in the dissipation basin slab during the first phase of operation. The variation indicated by the arithmetical sign of normal stress occurs alternately with along the basin slab. The spillway monolith is subject to lower stress values – these are mainly compressive. Layers of compressive and tensile stresses are formed mainly in the second phase – the tensile stresses occur in the spillway monolith in the foundation section and the compressive stresses occur in the area near the surface; tensile stresses prevail in the dissipation basin slab. The flip bucket is subject to compressive stresses in both phases of variation of the conditions.

References

[1] Brebbia C.A., *Fluid Structure Interaction V. Wessex Institute of Technology*, UK, WITpress, Southhampton, Boston 2009.

[2] Hammack E. Allen, Fong Moira T., Stockstill Richard L., *Calculating Forces on Components of Hydraulic Structure*, US Army Corps of Engineers, ERDC/CHL CHETN-IX-21, August 2009.

[3] Bandringa H., *Immersed boundary methods, Institute of Mathematics and Computing Science*, University of Groningen, August 2010.
[4] Peskin Charles S., *The immersed boundary method,* Acta Numerica, 2002, 479–517c, Cambridge University Press, DOI: 10.1017/S0962492902000077.
[5] Hou G., Wang Jin, Layton A., *Numerical Methods for Fluid-Structure Interaction – A Review*, Commun. Comput. Phys., Vol. 12, No. 2, pp. 337-377, August 2012, DOI: 10.4208/cicp.291210.290411s.
[6] Kostecki S., Rędowicz W., *The Washout Mechanism of the Niedów Dam and its Impact on the Parameters of the Flood Wave*, Procedia Engineering, 91, Wrocław 2014, 292–297, DOI: 10.1016/j.proeng.2014.12.062.
[7] Twaróg B., Failure *of Dam Niedów in Poland Preliminary Analysis and Conclusions*, Flow 3D Americas Users Conference, Canada, Toronto 2014.
[8] Twaróg B., *Katastrofa zapory Niedów – modelowanie z wykorzystaniem FLOW-3D, Wybrane problemy planowania i zarządzania w warunkach kryzysowych*, Chapter: II. *Wybrane narzędzia wspierające proces podejmowania decyzji (Selected tools supporting the decision-making process)*, M. Maciejewski, T. Walczykiewicz (eds.), IMGW PIB Poland, 95–106.